

Discrete-step evaporation of an atomic beam

T. Lahaye and D. Guéry-Odelin

Laboratoire Kastler Brossel^a, Département de Physique de l'École Normale Supérieure,
24 rue Lhomond, 75005 Paris, France

March 23, 2002

Abstract. We present a theoretical analysis of the evaporative cooling of a magnetically guided atomic beam by means of discrete radio-frequency antennas. First we derive the changes in flux and temperature, as well as in collision rate and phase-space density, for a single evaporation step. Next we show how the occurrence of collisions during the propagation between two successive antennas can be probed. Finally, we discuss the optimization of the evaporation ramp with several antennas to reach quantum degeneracy. We estimate the number of antennas required to increase the phase-space density by several orders of magnitude. We find that at least 30 antennas are needed to gain a factor 10^8 in phase-space density.

PACS. 32.80.Pj, 39.25.+k, 05.30.Jp

1 Introduction

Evaporative cooling [1] is so far the only technique allowing the achievement of quantum degeneracy in dilute gases. Several models of evaporative cooling of a trapped cloud of atoms have been studied. They are based either on approximating the cooling process as a series of truncations of the distribution function followed by rethermalization [2], or on an approximate analytical solution of the Boltzmann equation [3].

With the achievement of Bose-Einstein condensation (BEC), the possibility of realizing sources of coherent matter waves has arisen. These "atom lasers" [4] open the way to fascinating applications in atom optics and interferometry. To date, all atom lasers have been achieved in a pulsed mode: coherent streams of atoms were extracted from a Bose-Einstein condensate until it was completely depleted. As a first step towards the realization of a cw atom laser, a continuous source of Bose-Einstein condensed atoms was created by periodically replenishing a condensate held in an optical dipole trap with new condensates [5]. This approach, in combination with an appropriate outcoupler, would lead to a cw atom laser.

Alternatively, the authors of [6] study the evaporation of an atomic beam propagating in a magnetic guide. They use an approximate solution of the Boltzmann equation based on a truncated gaussian ansatz [3]. This approach permits the establishment of a set of hydrodynamic-like equations which is solved numerically. This treatment however can be made rigorous only for a one-dimensional evaporation. It would describe correctly evaporation on a dielectric surface on which atoms can be adsorbed [7].

From an experimental point of view, the propagation of a single packet of atoms has been realized in both macroscopic and microscopic atom guides [8,9,10,11,12,13,14,15]. More recently, a continuous magnetically guided beam was achieved, by directly injecting a beam of cold atoms generated by a moving molasses magneto-optical trap [16] as well as by feeding a magnetic guide periodically at a high repetition rate [17]. A first step of evaporation on this continuous guided beam has even been carried out by means of a single radio-frequency antenna. A natural way to attain degeneracy consists in using several radio-frequency (RF) antennas with decreasing frequencies. It would be the analog in space of the time-dependent RF ramp used in standard BEC experiments. The major difference lies in the fact that the evaporative cooling is ensured by successive cycles of evaporation followed by rethermalization.

In this work, we present the corresponding discrete model of evaporation by successive antennas. The two-dimensional character of the confinement allows us to derive analytical expressions that can be directly compared to experiments. After describing the magnetic guide in which atoms propagate, we derive how a single evaporation step affects the parameters of the beam (flux, temperature) and we deduce how the elastic collision rate within the beam, as well as the on-axis phase-space density, evolve. We then show how one can characterize the occurrence of rethermalization between two successive antennas as was demonstrated experimentally in [17]. We finally address the issue of the optimization of the evaporation ramp with many antennas.

^a Unité de Recherche de l'École Normale Supérieure et de l'Université Pierre et Marie Curie, associée au CNRS.

2 Magnetic guide

Quadrupole guides can be produced by means of four wires or tubes equally spaced on a cylinder of radius a and carrying currents $+I$ and $-I$ alternatively. The cylindrical symmetry axis is chosen to be the z -axis in the following. The resulting magnetic field is well approximated by a linear form: $B(r) = br$ where $r = (x^2 + y^2)^{1/2}$ is the distance from the z -axis and $b = 2 \mu_0 I / (a^2)$ is the transverse gradient. In this quadrupolar configuration, atoms with low angular momentum are not stable against spin flips. To counteract this loss mechanism, one superimposes a bias field B_0 along the axis of the guide [18]. As a consequence, the potential experienced by the low-field seeking atoms is:

$$U_g(x; y; z) = [B_0^2 + b^2 r^2]^{1/2}; \quad (1)$$

where μ_B is the magnetic moment of an individual atom.

In the following, we consider a beam of atoms of mass m , transversally confined by the potential (1), with a mean velocity v , a temperature T , and a flux Φ .

At equilibrium the thermal average of U_g is:

$$\langle U_g \rangle_T = \frac{\int_0^{R_1} U_g e^{-U_g/r} dr}{\int_0^{R_1} e^{-U_g/r} dr} = k_B T \left(2 + \frac{2}{1 + \frac{2}{1 + \frac{2}{1 + \dots}}} \right); \quad (2)$$

where $\mu_B = 1/k_B T$ and $\mu_B = B_0/k_B T$. For rubidium 87 polarized in the low-field seeking state of the lowest hyperfine level $F = m_F = 1$, $\mu_B = 2$ where μ_B is the Bohr magneton, and $\mu_B = 1$ with $B_0 = 1$ Gauss for a temperature of $T = 34$ K.

In the context of evaporative cooling, two quantities are of interest: The on-axis phase-space density D and the elastic collision rate γ_{coll} . For the potential (1) we readily obtain

$$D = \frac{1}{2} \frac{1}{1 + \frac{2}{v}} \frac{b}{k_B T} \frac{h^3}{(2 m k_B T)^{3/2}}; \quad (3)$$

Assuming that the elastic collision cross-section is constant the collision rate reads:

$$\gamma_{coll} = \frac{1}{2} \frac{1 + 2}{(1 + \frac{2}{v})^2} \frac{b}{k_B T} \frac{2 r}{m} \frac{k_B T}{m}; \quad (4)$$

Two limits are of interest depending on the value of μ_B . In the low temperature regime ($\mu_B \gg 1$), one can perform a Taylor expansion of (1) resulting in the harmonic form with an energy offset B_0 :

$$U_g(x; y; z) \approx B_0 + \frac{1}{2} m \omega^2 r^2; \quad (5)$$

and angular frequency $\omega = [b^2/(m B_0)]^{1/2}$. The thermal potential energy (2) reduces to $B_0 + k_B T$, and D (resp. γ_{coll}) scales with ω and T as $T^{-5/2}$ (resp. $T^{-1/2}$). In the opposite limit, where $\mu_B \ll 1$ one deals with a linear potential: $U_g(x; y; z) \approx br$. The thermal potential energy is $\langle U_g \rangle_T = 2k_B T$, and the scalings for D and γ_{coll} are $T^{-7/2}$ and $T^{-3/2}$.

3 Evaporation with one antenna

In order to perform evaporation on the beam, one uses an RF antenna to produce an oscillating magnetic field at a frequency ν_{RF} . Atoms whose trajectories cross the cylinder of axis z and radius R , defined by $h \nu_{RF} = U_g(R)$, will be resonant with the RF field and undergo a spin flip transition to an untrapped state. They are therefore removed from the atomic beam, whose flux decreases to the new value Φ_0 .

We define the evaporation parameter as $\alpha = h(\nu_{RF} - \nu_0)/k_B T$, where $\nu_0 = U_g(0)/h$ is the frequency corresponding to the bottom of the trap. In the following we first calculate, as a function of α , the fraction $f(\alpha) = \Phi_0/\Phi$ of remaining atoms after such an evaporation cycle. The distribution function of the atoms just after evaporation is out of equilibrium. Assuming subsequent rethermalization of the beam, we then calculate its new temperature T^0 . In this paper we assume that the collision rate γ_{coll} is much smaller than the typical period of oscillation (radial collisionless regime). In other words, we assume that particles do not undergo collisions over the range of efficiency of a radio frequency antenna. Therefore, determining if a particle will be evaporated or not depends only on the characteristics of its trajectory.

3.1 Fraction $f(\alpha) = \Phi_0/\Phi$ of remaining atoms

To calculate $f(\alpha)$, we need to know the fraction of atoms in the beam whose trajectories in the (xy) plane cross the circle of radius R .

3.1.1 Effective potential

The confining potential U_g being cylindrically symmetric, the z component L of angular momentum is conserved. To study the radial motion of an atom, one therefore uses the effective one-dimensional potential

$$U_e(L; r) = U_g(r) + \frac{L^2}{2m r^2} \quad (6)$$

which includes the centrifugal term. The radial coordinate $r(t)$ of the particle oscillates between the turning points r_{min} and r_{max} . The atom is evaporated if and only if $r_{min} \leq R \leq r_{max}$, or equivalently if its transverse energy E_{\perp} fulfills $E_{\perp} > U_e(R)$ (see Fig. 1). As a consequence, the evaporation criterion depends on the two constants which define completely the characteristics of the transverse trajectory: the total mechanical transverse energy E and the angular momentum L along the z -axis.

3.1.2 Joint probability distribution of energy and angular momentum

We now determine, for a thermal distribution at temperature T in the potential U_g , the joint probability distribution $p(E; L)$ for an atom to have energy E and angular

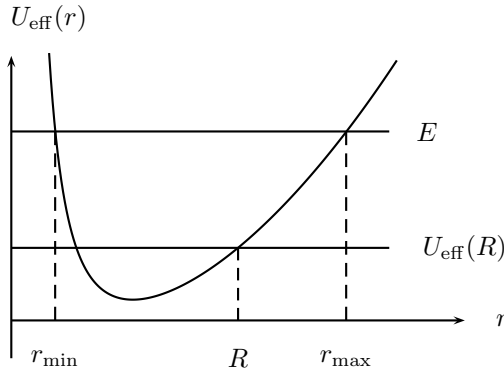


Fig. 1. Effective potential $U_{\text{eff}}(r)$. An atom with $E > U_{\text{eff}}(R)$ is evaporated.

momentum L . By definition

$$p(E; L) = C \int_0^{\infty} e^{-H(E, H_z)} (L - z) dz d^2p \quad (7)$$

where $H(r; p) = p^2/(2m) + U_g(r)$, $H_z = (p_z/m)$ and C is a normalization constant determined by $\int p(E; L) dE dL = 1$. The joint probability can be readily recast in terms of the period of the radial motion $T_r(E; L)$ [19]:

$$p(E; L) = C^0 e^{-E} T_r(E; L) \quad (8)$$

3.1.3 Harmonic confinement

For a harmonic confinement $U_g(r) = m \omega^2 r^2/2$, $T_r(E; L) = \pi \sqrt{2m(E - E_{\text{min}}(L))}$. The latter condition just reflects that a finite angular momentum requires a minimum energy which corresponds to the circular motion. We readily obtain the exact expression for the joint probability:

$$p_{\text{har}}(E; L) = \frac{1}{2(k_B T)^2} e^{-E} \Theta(E - E_{\text{min}}(L)); \quad (9)$$

where Θ is the Heaviside step function. The fraction of remaining atoms is given by [20]:

$$\bar{n}_{\text{har}}(R) = \int_{D(R)} p_{\text{har}}(E; L) dE dL = 1 - \frac{1}{2} e^{-E_{\text{min}}(R)} \quad (10)$$

The integration domain in Eq. (10) is defined by $D(R) = \{E, L \mid E \geq E_{\text{min}}(L), L \leq L_1(R)\}$ and corresponds to the shaded area in the plane $(E; L)$ depicted in Fig. 2. The subregion of $D(R)$ such that $L \leq L_1(R)$ (resp. $L > L_1(R)$) corresponds to trajectories not evaporated since $r_{\text{max}} < R$ (resp. $r_{\text{min}} > R$). The solid line in Fig. 3 represents $\bar{n}_{\text{har}}(R)$. For small R ($\ll 1$), few atoms have a sufficiently low angular momentum to be evaporated and $\bar{n}_{\text{har}} \ll 1$. For large R ($\gg 1$) the evaporative loss is negligible because of the exponential decay of the energy distribution and $\bar{n}_{\text{har}} \approx 1$. Between those two limits, the fraction of remaining atoms has a minimum for $\bar{n}_{\text{har}} = 0.5$ with $\bar{n}_{\text{har}}(R) \approx 0.24$.

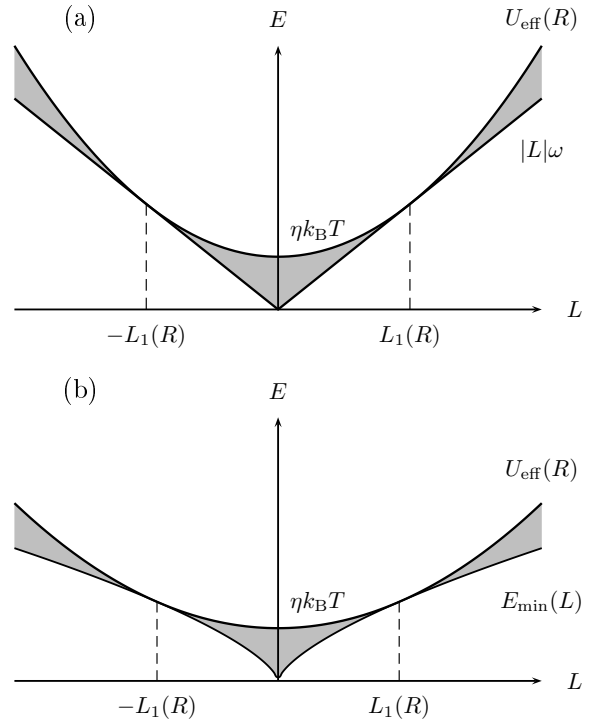


Fig. 2. Domain of integration $D(R)$ in the plane $(E; L)$. $L_1(R)$ is the angular momentum of a particle having a circular trajectory of radius R . (a): harmonic confinement (with $L_1(R) = m R^2 \omega$), (b): linear confinement (with $L_1(R) = m \omega R^3$).

3.1.4 Linear confinement

For linear confinement, the radial period $T_r(E; L)$ has no simple analytical expression. However, $T_r(E; L)$ has a weak dependence on the angular momentum L : for a given E , when L varies from 0 (linear trajectory) to its maximal value (circular trajectory), T_r varies by less than 10%. We therefore make the approximation $T_r(E; L) \approx T_r(E; 0) / E^{1/2}$ and approximate the joint distribution $p(E; L)$ by:

$$p_{\text{lin}}(E; L) \approx C E^{1/2} e^{-E} \Theta(E - E_{\text{min}}(L)); \quad (11)$$

The minimum value of E for a given L (energy of circular motion) is now: $E_{\text{min}}(L) = 3 \hbar^2 L^2 / (2m) = (2m)^{-1/3} L^2$. The fraction of remaining atoms can be written as $\bar{n}_{\text{lin}}(R) = \int_{D(R)} p_{\text{lin}}(E; L) dE dL$ where the integration domain is of the form $D(R) = \{E, L \mid E \geq E_{\text{min}}(L), L \leq L_1(R)\}$ (see Fig. 2). The result of the numerical integration based on the approximation (11) is plotted as a dashed line in Fig. 3. The shape is qualitatively the same as that for the harmonic confinement, but the minimum now occurs at $\bar{n}_{\text{lin}} \approx 1.25$ with $\bar{n}_{\text{lin}}(R) \approx 0.33$.

To check the validity of the approximation (11), we performed a Monte-Carlo sampling of the atomic distribution in a linear potential, followed by elimination of particles whose trajectories crossed the circle of radius R . The result for $\bar{n}_{\text{lin}}(R)$ is shown by dots in Fig. 3. The agreement is excellent.

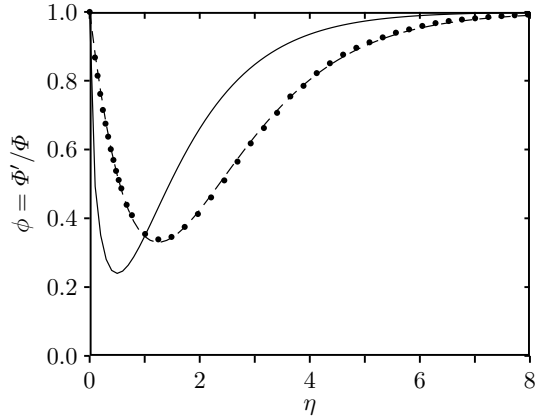


Fig. 3. Fraction $\phi = \Phi/\Phi_0$ of remaining atoms after evaporation by one antenna, as a function of the evaporation parameter η . Solid line: Harmonic confinement; dashed line: Linear confinement, being calculated with the approximation (11); dots: Linear confinement, being calculated by a Monte-Carlo simulation.

It is convenient in practice to have a simple form for the expression of $\phi_{\text{lin}}(\eta)$. Following the functional form of (10), we fit the curve $\phi_{\text{lin}}(\eta)$ by a function of the form $1 - a e^{-b\eta} + c$ where a, b, c are adjustable parameters and $a = 1.65, b = 1.13$ and $c = 0.92$. The curve obtained this way differs from $\phi_{\text{lin}}(\eta)$ by less than 2%. This simple expression is used in [17] to fit the experimental data, with the temperature T of the beam being the only adjustable parameter.

3.2 Temperature change $T^0 = T$

Consider N atoms undergoing evaporation by one antenna. After evaporation the total transverse energy of the $N^0 = \phi(\eta)N$ remaining atoms is given by:

$$E_{\perp}^0 = N \int_0^{\infty} \int_0^{\infty} E p(E; L) dE dL = N k_B T g(\eta); \quad (12)$$

where $\eta = 2$ for a harmonic potential and $\eta = 3$ for a linear potential. The dimensionless function $g(\eta)$ introduced in Eq. (12) can be calculated analytically for the harmonic confinement:

$$g_{\text{har}}(\eta) = 1 - \frac{(\eta)^{1/2}}{4} (3 + 2\eta) e^{-\eta}; \quad (13)$$

For a linear confinement, $g_{\text{lin}}(\eta)$ is calculated numerically thanks to the approximation (11).

The total (transverse and longitudinal) energy of the remaining atoms is $E^0 = E_{\perp}^0 + N^0 k_B T = 2 + N^0 m v^2 = 2$. After rethermalization (which occurs at constant total energy), one has an equilibrium state with a temperature T^0 and energy $E^0 = (\eta + 1/2) N^0 k_B T^0 + N^0 m v^2 = 2$. The relative change of temperature during this evaporation-rethermalization cycle is therefore:

$$\tau = \frac{T^0}{T} = \frac{1}{2 + \eta} \left(1 + 2 \frac{g(\eta)}{\phi(\eta)} \right); \quad (14)$$

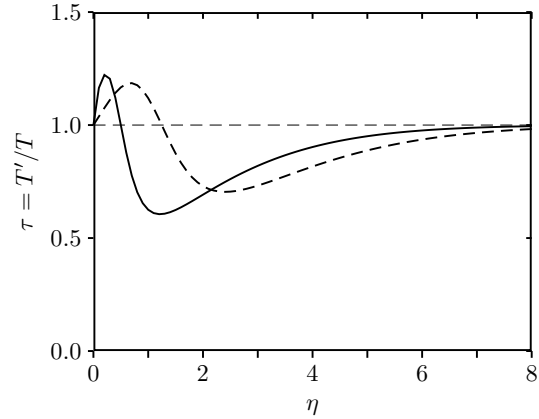


Fig. 4. Temperature change $\tau = T^0/T$ after evaporation by one antenna and rethermalization, as a function of η . Solid line: harmonic confinement; dashed line: linear confinement.

In Fig. 4, $\tau(\eta)$ is plotted as a function of η (solid line: harmonic case, dashed line: linear case). For low η (approximately lower than the value for which τ reaches a minimum), $T^0 > T$: since essentially low energy atoms are evaporated, the remaining beam acquires a higher temperature after rethermalization. The opposite occurs for high η : the beam is cooled by evaporation of high energy particles.

3.3 Variation of collision rate and phase-space density

After an evaporation followed by a subsequent rethermalization, the flux is multiplied by a factor ϕ , and the beam temperature is T^0 . We can then calculate, using Eqs. (3) and (4), the new phase-space density D^0 and the new collision rate ϕ_{coll}^0 .

The variation in phase-space density $\phi = D^0/D$ is plotted as a function of η in Fig. 5 (solid line: harmonic case; dashed line: linear case). For a linear confinement an increase of D is obtained as soon as $\eta > 2$, and for $\eta' \geq 3.0$ a maximum gain in phase-space (by a factor 1.86) can be achieved with a single antenna. The gain is less significant in the case of a harmonic confinement, reflecting the less favorable scaling law.

In order for evaporative cooling to be efficient, the elastic collision rate must not decrease during the process, otherwise the time needed for rethermalization becomes prohibitively long. Fig. 6 depicts the variation of collision rate $\phi(\eta) = \phi_{\text{coll}}^0 / \phi_{\text{coll}}$ for one evaporation cycle. The striking result is that in the case of harmonic confinement the collision rate cannot increase significantly (ϕ reaches a maximum value of 1.0015 for $\eta = 6.5$). This behaviour is due to the two-dimensional geometry of the problem and does not hold for a three-dimensional harmonic confinement. In contrast, for a linear guide, and for η sufficiently high, the collision rate can increase by several percent at each cycle, creating the possibility of runaway evaporation. This salient feature of the linear potential is well known for three-dimensional evaporative cooling [1,2].

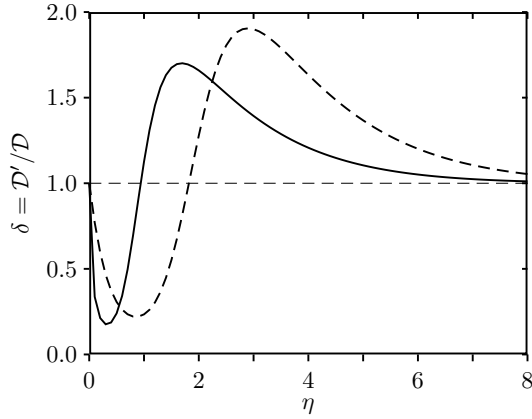


Fig. 5. Gain in phase-space density \mathcal{D}'/\mathcal{D} after evaporation by one antenna and rethermalization, as a function of η . Solid line: harmonic confinement; dashed line: linear confinement.

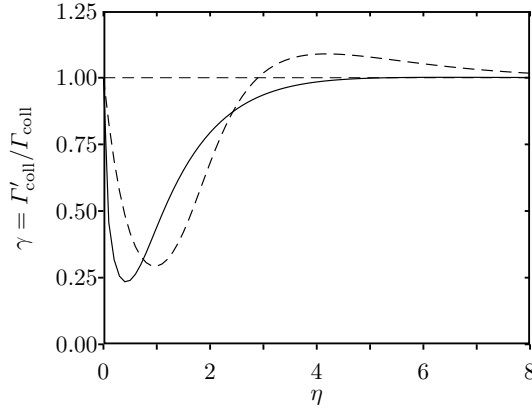


Fig. 6. Variation of the collision rate after evaporation by one antenna and rethermalization, as a function of η . Solid line: harmonic confinement; dashed line: linear confinement.

3.4 Multi-radius evaporation

The previous evaporation method has the disadvantage that for any finite η , some atoms with large energy and angular momentum are not evaporated. The contribution of these atoms to the energy of the truncated distribution is not negligible, and therefore the cooling efficiency of the evaporation is limited.

In order to improve this efficiency, one can evaporate all the atoms whose trajectories lie, at least partially, outside of the cylinder of radius R . To realize such an evaporation, one must use a "continuum" of evaporation radii $R \in [R_1; R_2]$. In practice, this can be achieved by scanning the radio-frequency ν_{RF} from $U_g(R) = \hbar \nu_{\text{RF}}$ to a value large compared to $k_B T = \hbar \nu_{\text{RF}}$, above which the population of atoms is exponentially small. The scanning rate must be large compared to the inverse of the time t_{ev} spent by an atom in the range of efficiency of an antenna, and small compared to the inverse of the mean radial period $T_r(E; L)$. For the typical parameters of the experiment described

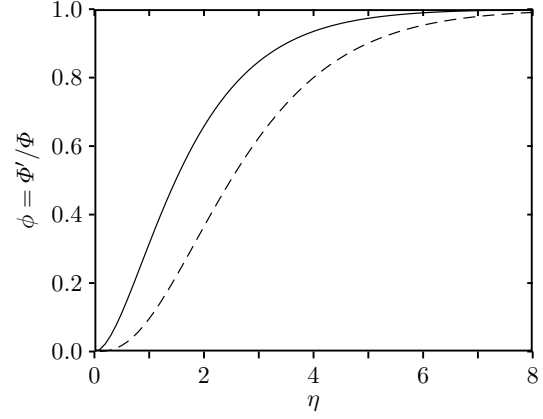


Fig. 7. Fraction $\phi = \Phi'/\Phi$ of remaining atoms after evaporation by one antenna, as a function of η , for the multi-radius evaporation scheme. Solid line: harmonic confinement; dashed line: linear confinement.

in [17], a scanning frequency of 50 Hz would fulfill both criteria.

One can calculate, in a way similar to the calculations of the previous subsections, the change in atomic flux $\Phi(\eta) = \Phi'_0$, in temperature $T(\eta) = T^0 = T$, in phase-space density $\mathcal{D}(\eta) = \mathcal{D}'/\mathcal{D}$, and in collision rate $\gamma(\eta) = \gamma'_0/\gamma_0$, for this improved evaporation scheme. The domain of integration is that shown in Fig. 2 but reduced to the angular momentum lower than $L_1(R)$. In the case of harmonic confinement, the calculations can be done explicitly and yield the following results:

$$\begin{aligned} \Phi(\eta) &= 1 - e^{-\eta^2} \quad (\eta^2 = 2e^{-\eta^2} \text{erf}(\eta^2)); \\ \gamma(\eta) &= 1 - (1 + \eta^2)e^{-\eta^2} \\ &\quad (3 + 4\eta^2 + \eta^4)e^{-\eta^2} \text{erf}(\eta^2) \quad (15) \end{aligned}$$

where $\text{erf}(x) = \frac{2}{\sqrt{\pi}} \int_0^x e^{-t^2} dt$ is the error function. The complete results for Φ , T , and γ and for both types of confinement are plotted in Figs. 7 to 10. Obviously, with this new evaporation scheme, the number of atoms remaining vanishes when $\eta \rightarrow 0$. The temperature change (Fig. 8) is now a monotonous function of η and for $\eta \rightarrow 0$, in the harmonic (resp. linear) case one has $T \rightarrow 1/5$ (resp. $1/7$) since only the longitudinal kinetic energy contributes to the energy of the remaining particles.

For a linear potential, the gain in phase-space density without decrease in collision rate is 2.56 (at $\eta = 2.5$) as compared to 1.86 (at $\eta = 3.0$) in the single radius evaporation scheme.

4 Evaporation with two antennas

The presence of elastic collisions in the atomic beam can be probed with a two-antenna experiment [17]. A first antenna with frequency ν_1 evaporates the atoms with an evaporation parameter $\eta_1 = \hbar \nu_1 / (k_B T)$, where T is the initial temperature of the atoms. The remaining flux is $\Phi^0 = \Phi(\eta_1)$. A second antenna with frequency $\nu_2 =$

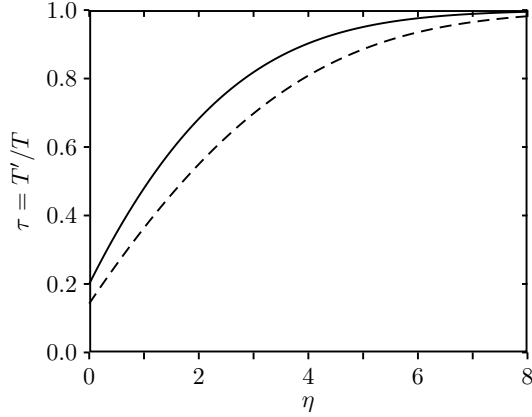


Fig. 8. Temperature change $\tau = T'/T$ after evaporation by one antenna and rethermalization, as a function of η , for the multi-radii evaporation scheme. Solid line: harmonic confinement; dashed line: linear confinement.

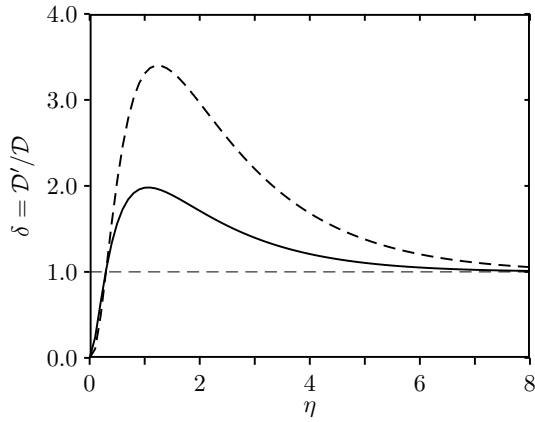


Fig. 9. Gain in phase space density after evaporation by one antenna and rethermalization, as a function of η , for the multi-radii evaporation scheme. Solid line: harmonic confinement; dashed line: linear confinement.

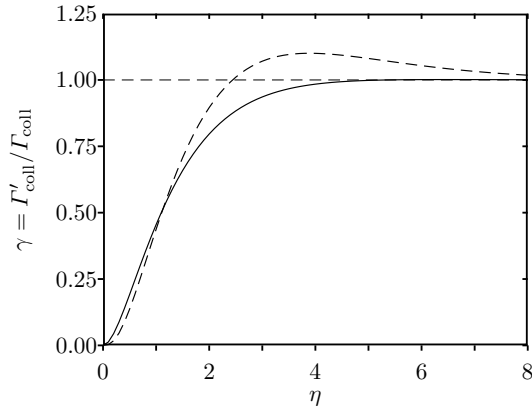


Fig. 10. Variation of the collision rate after evaporation by one antenna and rethermalization, as a function of η , for the multi-radii evaporation scheme. Solid line: harmonic confinement; dashed line: linear confinement.

$2k_B T = \hbar$, placed at a distance d downstream, is used to probe the distribution of atoms after this first evaporation stage. The flux after this second antenna is denoted ω . In the absence of collisions between the two antennas, the distribution remains out of equilibrium. In particular, if $\eta_2 = \eta_1$, the second antenna cannot remove extra atoms, since all atoms whose energy and angular momentum corresponded to the evaporation criterion have already been removed by the first antenna. But even a partial rethermalization leads to some extra losses from the second antenna, since elastic collisions provide a redistribution of energy and angular momentum. If the beam completely rethermalizes during its propagation between the two antennas, we find a spectrum similar to that of Fig. 3 revealing the new temperature T^0 .

4.1 In absence of collisions

We calculate here the fraction $\omega = \omega^0$ in the limit where rethermalization does not occur between the two antennas, i.e. when the inequality $\text{coll} \ll v$ is fulfilled. After evaporation by the first antenna at η_1 (corresponding to an evaporation radius R_1), the out of equilibrium joint probability distribution $p_1(E; L)$ of $(E; L)$ is given by

$$p_1(E; L) = p(E; L) \quad (U_e(R_1) \leq E) : \quad (16)$$

It is non-zero only in the domain $D_1 \subset D_2$ of Fig. 11. The fraction of remaining atoms $\omega = \omega^0$ is therefore given by integrating (16) over the domain $D_2 = \int_{E_{\min}(L)}^{E_{\max}(L)} dE \int_{L_{\min}(E)}^{L_{\max}(E)} dL$:

$$\frac{\omega}{\omega^0} = \frac{\int_{D_2} p_1(E; L) dE dL}{\int_{D_1 \cup D_2} p_1(E; L) dE dL} : \quad (17)$$

The result of the numerical integration is shown in Fig. 12 as a dashed line, for the specific case of a linear confinement with $\eta_1 = 2$. As expected, the fraction $\omega = \omega^0$ reaches 1 for $\eta_2 = 2$.

4.2 Rethermalization

If rethermalization occurs over a distance d , that is if the collision rate is such that: $\text{coll} \gg v$, the second antenna evaporates a beam of temperature $T^0 = (\eta_1)T$ at thermal equilibrium. The fraction $\omega = \omega^0$ is therefore:

$$\frac{\omega}{\omega^0} = \frac{\hbar \eta_2}{k_B T^0} = \frac{\eta_2}{(\eta_1)} : \quad (18)$$

This curve is plotted as a solid line on Fig. 12. The large difference between the collisionless and collisional regimes makes it easy to detect experimentally, by scanning η_2 in the vicinity of η_1 , the presence or the absence of collisions within the beam [17].

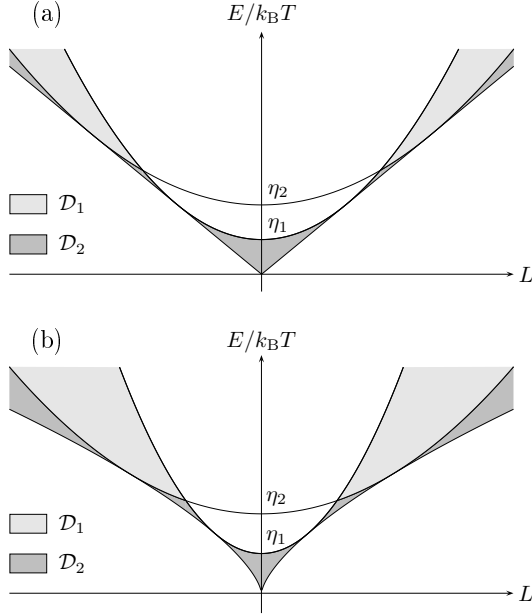


Fig. 11. The integration domains in the plane $(E; L)$ involved in the calculation of $\omega=0$ in the collisionless regime. (a): Harmonic confinement; (b): Linear confinement.

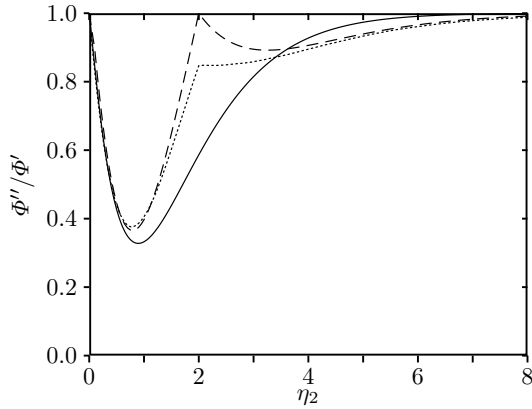


Fig. 12. Fraction $\omega=0$ of the flux remaining after the second antenna as a function of its parameter η_2 . The first antenna is driven at a frequency $\omega_1 = \eta_1 k_B T = \hbar$ with $\eta_1 = 2 = 1.6$. The dashed line corresponds to the collisionless regime; the dotted line to a mean number of collisions between antennas $N_c = 1.1$; the solid line to full rethermalization. These curves are calculated with a numerical simulation, in the case of a linear confinement.

4.3 Number of collisions required to thermalize

In order to give a quantitative theoretical account for the distance d needed to rethermalize in a two-antenna experiment, we have developed a numerical simulation of the motion of the atoms in the magnetic guide for both linear and harmonic confinements. We use a molecular dynamics simulation [21] taking into account the evaporation criterion.

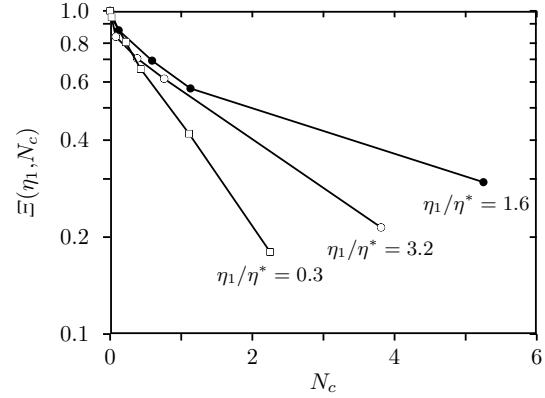


Fig. 13. Distance from equilibrium $\Xi(\eta_1; N_c)$ (see text) as a function of the mean number of collisions N_c between the two antennas, for different values of η_1 . These data have been obtained by a Monte-Carlo simulation performed for a linear confinement. The relaxation towards equilibrium is clearly exponential for $\eta_1 = 0.3$, and approximately exponential for $\eta_1 = 3.2$. For $\eta_1 = 1.6$, the first antenna puts the gas in a strongly out-of-equilibrium state, and the relaxation is not exponential.

The simulation is performed in dimensionless units. The unit length r_u is defined by $U_g(r_u) - U_g(0) = (\hbar U_g i_T - U_g(0)) = 2$, the distance between the two antennas is $d = 5000 r_u$. The mean velocity is 10 times the thermal velocity $(k_B T = m)^{1/2}$. The phase-space variables of each particle are evolved by advancing the position and the velocity at discrete time steps Δt according to a second-order symplectic integration [22]. Using the cylindrical symmetry we restrict the evolution to the first quarter ($x > 0, y > 0$) of space with reflecting walls at planes $x = 0$ and $y = 0$. Binary elastic collisions are taken into account using a boxing technique [23]. The constant cross section used to calculate the probability of collisions is adjusted to the desired number of collisions between the two antennas. Simulations have been performed with 1.5×10^6 particles and 5.4×10^4 boxes. The time step Δt is chosen to be small with respect to the typical collision timescale and the typical period of oscillation.

We simulate a two-antenna experiment in which the first antenna is operated at a fixed η_1 . The mean number of collisions per atom during the propagation between the two antennas is denoted N_c . The second antenna is operated at η_2 , and we calculate $\omega=0$ as a function of η_2 . An example of such a curve, for a linear confinement, and with $N_c = 1.1$, is plotted as a dotted line in Fig. 12.

We then infer the ratio $f(\eta_1; N_c) = \omega=0(\eta_2 = \eta_1)$ as a function of N_c . For a collisionless propagation ($N_c = 0$, dashed line in Fig. 12), we have $f(\eta_1; 0) = 1$. For a complete rethermalization, ($N_c \rightarrow 1$, solid line in Fig. 12), the ratio tends to the limit $f_1(\eta_1) = [\eta_1 = (\eta_1)]$.

For a linear confinement, we depict in Fig. 13 the normalized quantity

$$(\eta_1; N_c) = \frac{f(\eta_1; N_c) - f_1(\eta_1)}{1 - f_1(\eta_1)};$$

which measures the distance from equilibrium, as a function of the mean number of collisions N_c . For a given γ_1 and in the absence of collisions $N_c = 0$, $\gamma = 1$. The relaxation of γ towards zero with increasing number of collisions N_c reflects the rethermalization process. For $\gamma_1 < 0.3$ or $\gamma_1 > 2.5$, γ decays approximately in an exponential manner with N_c : $\gamma \sim \exp[-N_c/n_c(\gamma_1)]$. As an example we find $n_c(4) = 2.5$ and $n_c(2) = 1.3$ for the harmonic confinement and $n_c(2) = 1.3$ and $n_c(4) = 0.2$ for the linear confinement. For intermediate values of the ratio $\gamma_1 = \gamma$, we obtain a non-exponential decay (see Fig. 13 for $\gamma_1 = 1.6$). In this range $0.3 < \gamma_1 < 2.5$, more than 50% of the atoms are evaporated by the first antenna, leading to a state of gas that is very far from equilibrium.

This calibration by numerical simulation allows one to determine the collision rate by following the thermalization process for different distances between the two antennas [17].

5 Evaporation with many antennas

The realization of a magnetically guided atomic beam in the collisional regime has recently been performed [17]. The phase-space density of this beam is on the order of 2×10^8 . To gain the 8 orders of magnitude required to reach degeneracy one can implement evaporative cooling by means of several successive antennas. In this section we assume that the frequency of each antenna is such that the parameter γ is constant throughout the evaporation.

The number of antennas $N(\gamma)$ required to achieve a gain γ in phase-space is, for a given value of γ , $N(\gamma) = \ln(\gamma) = \ln(\gamma_1)$. We want to minimize the guide length needed to reach degeneracy. This length $L(\gamma)$ can be evaluated from the initial collision rate of the beam γ_{coll}^0 . Between the antennas n and $n+1$, the collision rate is γ_{coll}^n . If the number of collisions required for full thermalization between two successive antennas is N_0 ($N_0 = n_c(\gamma)$), the distance between antennas n and $n+1$ has to be larger than $vN_0 = (\gamma_{coll}^0)^{-1}$. Therefore the total length is

$$L(\gamma) > \frac{vN_0}{\gamma_{coll}^0} (1 + \gamma^{-1} + \gamma^{-2} + \dots + \gamma^{-N(\gamma)}) \\ > \frac{vN_0}{\gamma_{coll}^0} \frac{1 - \gamma^{-N(\gamma)+1}}{1 - \gamma^{-1}} : \quad (19)$$

For a given value of γ , there exists an optimal choice γ^* for the parameter γ such that L is minimized. For this optimization we assume that N_0 does not depend on γ . The results are shown, for both types of confinement and for the two evaporation schemes, in Table 1. The evaporation is much less efficient for the harmonic confinement, which reflects the absence of runaway evaporation for this type of trap. For the linear confinement, one sees that the multi-radii evaporation scheme leads to a slightly shorter evaporation length, at the expense of a reduced output flux. However a more careful study shows that for comparable output fluxes, the two schemes require approximately the same length and antenna numbers. In the case

Scheme	Single radius		Multi-radii	
	Har	Lin	Har	Lin
γ_{min}	211	12.0	211	10.5
\sim	4.6	4.3	4.6	3.6
N	142	42	142	29
$\gamma_f = \gamma_i$	$3.9 \cdot 10^{-3}$	$5.4 \cdot 10^{-4}$	$3.9 \cdot 10^{-3}$	$1.3 \cdot 10^{-4}$
$T_f = T_i$	$6.9 \cdot 10^{-5}$	$6.0 \cdot 10^{-4}$	$6.9 \cdot 10^{-5}$	$3.8 \cdot 10^{-4}$

Table 1. Parameters of the optimized (minimum length) evaporation ramp for harmonic (Har) and linear (Lin) confinements, for the two schemes of evaporation, with a total gain in phase-space density of $\gamma = 10^8$: γ_{min} , evaporation length (in units of $vN_0 = (\gamma_{coll}^0)^{-1}$); \sim , parameter for minimal evaporation length; N , number of antennas needed; $\gamma_f = \gamma_i$, total flux reduction due to evaporation; $T_f = T_i$, total temperature reduction due to evaporation.

of harmonic confinement, since the collision rate cannot increase significantly, minimizing the evaporation length requires that one operates at a large γ (where $\gamma \gg 1$). For such high γ , the difference between the two evaporation schemes is negligible, as can be seen in Table 1.

In this paper, two competing effects that should be considered in a more realistic model of the evaporation ramp have been neglected. First, the real shape of the semi-linear potential (1) should be taken into account. Indeed, even if at the beginning of the evaporation ramp the temperature is high enough for the linear potential to be a good approximation ($\gamma \gg 1$), as the temperature is reduced the effect of the bias field cannot be neglected anymore when $\gamma \sim 1$. This effect may lead to a longer evaporation length since, for the harmonic confinement, the evaporative cooling is less efficient. The second effect, neglected by the classical description used in this paper, is the bosonic stimulation close to degeneracy, which might enhance the efficiency of the last evaporation steps.

6 Conclusion

We have studied theoretically the discrete-step evaporative cooling of a magnetically guided atomic beam. First, the action of a single antenna on the beam is analyzed in detail. Then we clarify how two-antenna experiments can lead (i) to the characterization of the collisional regime of the beam and (ii) to the quantitative estimate of the collision rate, by studying the number of collisions needed for thermalization of the truncated distribution function. Finally, the problem of optimizing the evaporation ramp with many antennas is addressed. We find that gains in

phase-space density of 10^8 require a total of at least 30 evaporation steps.

We are indebted to J. Dalibard for useful comments and to P. Cren for the development of a preliminary version of the numerical simulation. We acknowledge stimulating discussions with J. M. Vogels, K. J. Gunter, K. Kozłowski and the ENS laser cooling group. We thank D. Roberts for careful reading of the manuscript. This work was partially supported by the CNRS, the Region Ile-de-France, the French Ministry of Research, the College de France, the Ecole Normale Supérieure, the Bureau National de la Métrologie, the University of Paris VI and the Délégation Générale de l'Armement.

References

1. W. Ketterle and N. J. Van Druten, *Adv. At. Mol. Opt. Phys.* **37**, 181, (1996).
2. K. B. Davis, M. -O. Mewes, W. Ketterle, *Appl. Phys. B* **60**, 155 (1995).
3. O. J. Luiten, M. W. Reynolds, and J. T. M. Walraven, *Phys. Rev. A* **53**, 381 (1996).
4. M. -O. Mewes, M. R. Andrews, D. M. Kum, D. S. Durfee, C. G. Townsend, and W. Ketterle, *Phys. Rev. Lett.* **78**, 582 (1997); I. Bloch, T. W. Hansch and T. Esslinger, *ibid* **82**, 3008 (1999); E. W. Hagley, L. Deng, M. Kozuma, J. Wen, K. Helmerson, S. L. Rolston, and W. D. Phillips, *Science* **283**, 1706 (1999); Y. Le Coq, J. H. Thywissen, S. A. Rangwala, F. Gebier, S. Richard, G. Delannoy, P. Bouyer, and A. Aspect, *Phys. Rev. Lett.* **87**, 170403 (2001).
5. A. P. Chikkatur, Y. Shin, A. E. Leanhardt, D. Kielpinski, E. T. Sikata, T. L. Gustavson, D. E. Pritchard and W. Ketterle, *Science* **296**, 2193 (2002).
6. E. Mandonnet, A. Minguzzi, R. Dum, I. Carusotto, Y. Castin and J. Dalibard, *Eur. Phys. J. D* **10**, 9 (2000).
7. D. M. Harber, J. M. McGuirk, J. M. Obrecht and E. A. Cornell, *J. Low Temp. Phys.* **133**, 229 (2003).
8. J. Schmiedmayer, *Phys. Rev. A* **52**, R13-R16 (1995).
9. J. Denschlag, D. Cassettari, and J. Schmiedmayer, *Phys. Rev. Lett.* **82**, 2014 (1999).
10. A. Göpfert, F. Lison, R. Schutze, R. Wynands, D. Haubrich, and D. Meschede, *Appl. Phys. B* **69**, 217 (1999).
11. M. Key, I. G. Hughes, W. Rooijakkers, B. E. Sauer and E. A. Hinds, D. J. Richardson and P. G. Kazansky, *Phys. Rev. Lett.* **84**, 1371 (2000).
12. N. H. Dekker, C. S. Lee, V. Lorent, J. H. Thywissen, S. P. Smith, M. D. Mdic, R. M. W. Estervelt, and M. Prentiss, *Phys. Rev. Lett.* **84**, 1124 (2000).
13. B. K. Teo and G. Raithel, *Phys. Rev. A* **63**, 031402 (2001).
14. J. A. Sauer, M. D. Barrett, and M. S. Chapman, *Phys. Rev. Lett.* **87**, 270401 (2001).
15. E. A. Hinds and I. G. Hughes, *J. Phys. D: Appl. Phys.* **87**, R119, (1999).
16. P. Cren, C. F. Roos, A. Aclan, J. Dalibard and D. Guéry-Odelin, *Eur. Phys. J. D* **20**, 107 (2002).
17. T. Lahaye, J. M. Vogels, K. J. Gunter, Z. Wang, J. Dalibard, and D. Guéry-Odelin, *Phys. Rev. Lett.* **93**, 093003 (2004).
18. If one superimposes a constant magnetic field over a three-dimensional quadrupole, there is always a point where the modulus of the magnetic field vanishes. By contrast, if the constant magnetic field has a non zero component on the axis of the two-dimensional quadrupole configuration of a magnetic guide, the resulting field never vanishes.
19. $T_r(E; L) = 2 \int_{r_{min}}^{r_{max}} dr = \frac{L}{2m} \int_{r_{min}}^{r_{max}} \frac{dr}{v(r)}$ where $v(r) = \sqrt{2m(E - U_g(r))}$ is the radial velocity of the atom.
20. C. F. Roos, P. Cren, T. Lahaye, J. Dalibard and D. Guéry-Odelin, *Laser Phys.* **13**, 605 (2003).
21. G. A. Bird, *Molecular Gas Dynamics and the Direct Simulation of Gas Flow*, Clarendon, Oxford, 1994.
22. B. Jackson and E. Zaremba, *Phys. Rev. A* **66**, 033606 (2002).
23. H. Wu and C. J. Foot, *J. Phys. B: At. Mol. Opt. Phys.* **29**, L321 (1996); H. Wu, E. Arimondo and C. J. Foot, *Phys. Rev. A* **56**, 560 (1997); D. Guéry-Odelin, J. Soding, P. Desbiolles, J. Dalibard, *Opt. Expr.* **2**, 323 (1998).